Article

The Nonphysiological Reductant Sodium Dithionite and [FeFe] Hydrogenase: Influence on the Enzyme Mechanism

Maria Alessandra Martini, Olaf Rüdiger, Nina Breuer, Birgit Nöring, Serena DeBeer, Patricia Rodríguez-Maciá,* and James A. Birrell*

Cite This: *J. Am. Chem. Soc.* 2021, 143, 18159–18171

Read Online

ACCESS | Metrics & More | Article Recommendations | SI Supporting Information

ABSTRACT: [FeFe] hydrogenases are highly active enzymes for interconverting protons and electrons with hydrogen (H_2). Their active site H-cluster is formed of a canonical [4Fe-4S] cluster ([4Fe-4S]$_H$) covalently attached to a unique [2Fe] subcluster ([2Fe]$_H$), where both sites are redox active. Heterolytic splitting and formation of H_2 takes place at [2Fe]$_H$, while [4Fe-4S]$_H$ stores electrons. The detailed catalytic mechanism of these enzymes is under intense investigation, with two dominant models existing in the literature. In one model, an alternative form of the active oxidized state H_{ox}, named $H_{ox}H$, which forms at low pH in the presence of the nonphysiological reductant sodium dithionite (NaDT), is believed to play a crucial role. $H_{ox}H$ was previously suggested to have a protonated [4Fe-4S]$_H$. Here, we show that $H_{ox}H$ forms by simple addition of sodium sulfite (Na_2SO_3, the dominant oxidation product of NaDT) at low pH. The low pH requirement indicates that sulfur dioxide (SO_2) is the species involved. Spectroscopy supports binding at or near [4Fe-4S]$_H$, causing its redox potential to increase by ~60 mV. This potential shift detunes the redox potentials of the subclusters of the H-cluster, lowering activity, as shown in protein film electrochemistry (PFE). Together, these results indicate that $H_{ox}H$ and its one-electron reduced counterpart $H_{red}'H$ are artifacts of using a nonphysiological reductant, and not crucial catalytic intermediates. We propose renaming these states as the "dithionite (DT) inhibited" states H_{ox}-DT_i and H_{red}-DT_i. The broader potential implications of using a nonphysiological reductant in spectroscopic and mechanistic studies of enzymes are highlighted.
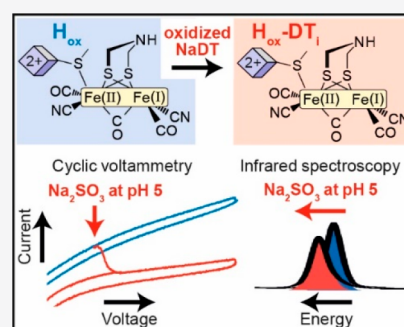
INTRODUCTION

[FeFe] hydrogenases are highly active metalloenzymes that catalyze the reversible reduction of protons to molecular hydrogen.[1,2] Their active site, the H-cluster, comprises a unique diiron subcluster ([2Fe]$_H$) and a canonical [4Fe-4S] subcluster ([4Fe-4S]$_H$), covalently linked by a cysteine thiolate[3,4] (Figure 1 A and B). The Fe of [2Fe]$_H$ that is closest to [4Fe-4S]$_H$ is known as the proximal Fe (Fe$_p$), while the Fe furthest from the cluster is known as the distal Fe (Fe$_d$). In [2Fe]$_H$, the Fe ions are coordinated by two terminal CN^- and two terminal CO ligands (one on each Fe), a bridging CO, and a bridging 2-azapropane-1,3-dithiolate (ADT) ligand.[5,6] During H_2 conversion, the H-cluster goes through a series of redox transitions, where the Fe ions change oxidation states, as well as protonation/deprotonation steps.[7–9] While several catalytic intermediate states have been well characterized with a variety of spectroscopic techniques, structural models based on X-ray diffraction data on crystals in spectroscopically defined states are not generally available. Thus, in the absence of structural models supported by experimental data, computational chemistry has played an important role in proposing likely structures of the active site in the catalytic intermediates based on spectroscopic data. However, divergent results from various groups have led to several possible models of the

catalytic cycle of [FeFe] hydrogenases.[8,10–12] These can be summarized in two main models (here referred to as Model 1 and 2, Figure 1C and D respectively).

The most oxidized state of the active enzyme, H_{ox}, is generally accepted to be the starting point of the catalytic cycle and has a mixed valence of Fe$_p$(II)Fe$_d$(I) in [2Fe]$_H$,[13] and an oxidized [4Fe-4S]$_H^{2+}$. In Model 1 (Figure 1C), one-electron reduction of H_{ox} is proposed to yield two possible states H_{red} and $H_{red}H^+$ (in our nomenclature), whose relative population depends on the pH. In H_{red}, the electron is thought to be localized preferentially on [4Fe-4S]$_H$. In $H_{red}H^+$, the electron is thought to be transferred to the [2Fe]$_H$ subcluster (with an Fe$_p$(I)Fe$_d$(I) configuration) and a proton (from the proton transfer pathway) to bind to the nitrogen in the ADT bridge giving an NH_2^+.[14,15] This process of proton-coupled electronic rearrangement (PCER) of the H-cluster is a crucial component of Model 1. A further one-electron reduction of $H_{red}H^+$ yields
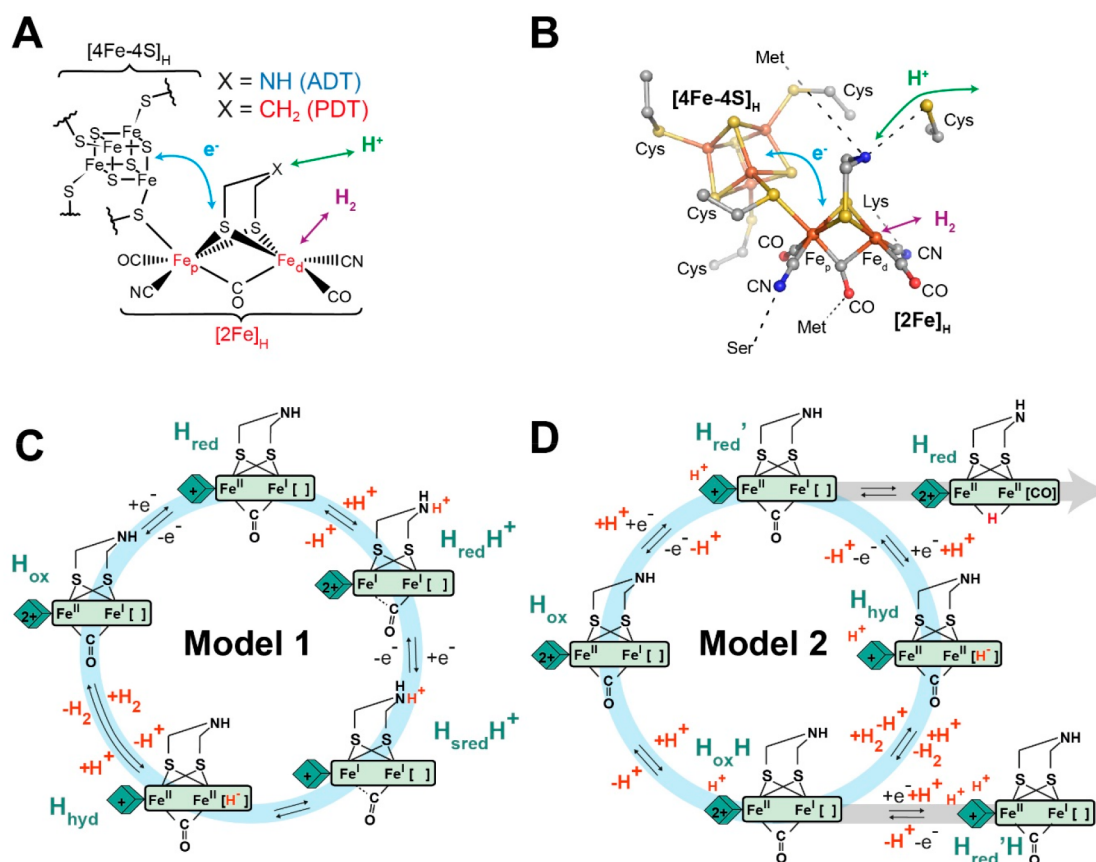
Figure 1. Structure of the H-cluster and proposed catalytic cycles. (A) Schematic showing the chemical structure of the $[2Fe]_H$ subcluster attached covalently to the $[4Fe-4S]_H$ subcluster. "X" in the bridgehead position is an NH group in the native ADT ligand and is CH_2 in the synthetic chemical variant PDT. (B) Structure of $[2Fe]_H$ and $[4Fe-4S]_H$ from HydA1 from *Clostridium pasteurianum* (PDB: 4XDC[26]) showing the nearby amino acids that interact with $[2Fe]_H$. (C) Catalytic cycle Model 1 in which one-electron reduction of $[4Fe-4S]_H$ is followed by proton-coupled electronic rearrangement to give the $H_{red}H^+$ state.[14] A further one-electron reduction of $[4Fe-4S]_H$ gives the $H_{sred}H^+$ state,[16] which is then followed by rearrangement to give the H_{hyd} state with a terminal hydride at Fe_d.[19−21] The subsequent steps leading to H_2 formation are not shown. (D) Catalytic cycle Model 2 in which proton-coupled electron transfer at $[4Fe-4S]_H$ converts H_{ox} to H_{red}', which can engage in further proton-coupled electron transfer to give the terminal hydride-containing H_{hyd} state.[10,19] H_{hyd} then reacts with an additional proton to generate H_2 leaving a protonated $H_{ox}H$ state.[27] Alternatively, H_{red}' can rearrange to give a less active H_{red} state containing a bridging hydride,[28] which proceeds through a low activity pathway. $H_{ox}H$ appears to undergo one-electron reduction to $H_{red}'H$, but this is not included in the catalytic cycle.[10,27]

the $H_{sred}H^+$ state with a reduced $[4Fe-4S]_H^+$.[16,17] The protonated ADT ligand in both $H_{red}H^+$ and $H_{sred}H^+$ appears to be able to transfer the proton to Fe_d generating an Fe-bound hydride in the H_{hyd} state.[18−23] Finally, the H_{hyd} state is thought to gain an additional proton, which may trigger a similar PCER process as in the H_{red} state, and form a H_2 molecule bound to Fe_d, which can then leave the enzyme via a hydrophobic gas channel.[24] Recently, photoexcitation of $H_{red}H^+$ and $H_{sred}H^+$ was shown to generate two different forms of H_{hyd}, known as $H_{hyd:ox}$ and $H_{hyd:red}$, where the former has an oxidized $[4Fe-4S]_H$ and the latter has a reduced $[4Fe-4S]_H$.[25]

In Model 2 (Figure 1D),[8] the H_{red} state (referred to as H_{red}') is formed from H_{ox} by proton-coupled electron transfer (PCET) at $[4Fe-4S]_H$. This was suggested based on IR spectroelectrochemical titrations at various pH values that showed a pH-dependent redox potential of $[4Fe-4S]_H$.[10] Specifically, the proton is thought to bind to one of the cysteine ligands coordinating the cluster. This state then undergoes an additional PCET at $[2Fe]_H$ to give the H_{hyd} state,[19] and the proton is retained on $[4Fe-4S]_H$. Hydrogen is then formed by additional protonation leaving an oxidized H-cluster but still protonated at $[4Fe-4S]_H$, a state called

$H_{ox}H$.[27] In Model 2, $H_{red}H^+$ (referred to as H_{red}) and $H_{sred}H^+$ (not shown in Figure 1D) contain a bridging hydride ($\mu H^−$) and an apical CO ligand,[28] and are considered to be part of a low activity pathway. Lastly, reduction of $H_{ox}H$ to $H_{red}'H$ has also been observed,[10] but its place in the catalytic cycle remains to be determined.

The $H_{ox}H$ and $H_{red}'H$ states in Model 2 have been reported to accumulate at low pH only in the presence of sodium dithionite (NaDT) (see Supporting Information for further details).[10,27] NaDT ($Na_2S_2O_4$, also sodium hydrosulfite) is widely used in biochemistry as an oxygen scavenger and low potential reducing agent ($E^{0'} = −0.66$ V vs SHE at pH 7 and 25 °C).[29] For example, it is commonly employed to protect metalloproteins from oxidative damage caused by trace amounts of oxygen during purification and handling, or to poise metallocofactors in reduced states for their characterization. However, one of the pitfalls of its use is the failure to consider that NaDT and its oxidation products can engage in side-reactions with the system under study. Several studies on sulfite-reducing enzymes have highlighted how oxidation of NaDT can be a significant source of $SO_3^{2−}$, the substrate for these enzymes, which can bind to the active site and

complicate the interpretation of spectroscopic studies and activity measurements.[30−32] In a recent report, during the semisynthetic assembly of the FeMo cofactor of nitrogenase, the donor of the ninth sulfur ligand was found to be the SO_3^{2-} generated by the oxidation or degradation of NaDT present in the assay.[33] Numerous studies have reported the interaction of oxidation products of NaDT with various enzymes including nitrite reductase,[34−36] DMSO reductase,[37] monomethylamine methyltransferase,[38] acetyl CoA synthase,[39] and formation of adducts to flavins[40−42] and cobalamin.[43,44] Additionally, the slow dissociation of NaDT into $SO_2^{\bullet-}$ radicals (the active reducing species) has been shown to be problematic in mechanistic studies of nitrogenase.[45]

In light of the dependence of $H_{ox}H$ and $H_{red}'H$ on NaDT, and of NaDT's reported "non-innocent" behavior, we decided to investigate the effect of NaDT and its oxidation products on [FeFe] hydrogenases. Formation of the $H_{ox}H$ state was observed when the [FeFe] hydrogenase from *Chlamydomonas reinhardtii* (*Cr*HydA1) was treated with oxidized NaDT. Addition of Na_2SO_3 (the dominant oxidation product of NaDT[46]) to *Cr*HydA1 at low pH reproduced the same effect as oxidized NaDT. Under H_2, $H_{red}'H$ was also observed. We propose that, at low pH, the dissolved sulfur dioxide (SO_2) generated by the protonation of SO_3^{2-} binds to the H-cluster. Based on our spectroscopic observations, we hypothesize that this occurs near $[4Fe-4S]_H$ with submicromolar binding affinity as estimated by IR titrations. Based on the ratios of the H_{ox}/H_{red} and $H_{ox}H/H_{red}'H$ states under H_2, binding of SO_2 causes the redox potential of $[4Fe-4S]_H$ to increase by ∼60 mV. The effect of this on catalysis was investigated via protein film electrochemistry (PFE), showing that binding of SO_2 has an inhibitory effect on both H^+ reduction and H_2 oxidation activity of [FeFe] hydrogenases. Together, these results reveal that the so-called $H_{ox}H$ and $H_{red}'H$ states are not related to protonation events at the $[4Fe-4S]_H$ subcluster of the H-cluster, but are instead artifacts generated by oxidized NaDT. This result challenges their involvement in the catalytic cycle of [FeFe] hydrogenases. Furthermore, these findings highlight the importance of carefully considering the possible side-reactions of NaDT and its oxidation products when choosing to use this reducing agent with metalloenzymes, particularly iron−sulfur enzymes.

■ RESULTS

Treatment of *Cr*HydA1 with oxidized NaDT causes formation of the HoxH state. Our investigation on the effect of the oxidation products of NaDT on [FeFe] hydrogenases focused, in the first instance, on *Cr*HydA1, the most well characterized [FeFe] hydrogenase, which contains only the H-cluster. In particular, the enzyme containing the native [2Fe] cofactor with the ADT ligand (*Cr*HydA1[ADT]) was used. Thus, *Cr*HydA1[ADT] produced in the strict absence of NaDT was treated with a solution of oxidized NaDT (oxNaDT). This solution was prepared by dissolving fresh NaDT in water to a concentration of 1 M (the most effective concentration of NaDT for $H_{ox}H$ formation at pH 6[27]) under aerobic conditions and stirring for 2 h under atmospheric oxygen. A decrease in the pH to ∼2 and appearance of a yellow precipitate (most likely elemental sulfur) indicated oxidation and degradation of the dithionite anion.[47] The oxNaDT solution was then thoroughly degassed and moved into an anaerobic glovebox before being added to *Cr*HydA1[ADT], in order to avoid damaging the highly air-sensitive H-cluster.
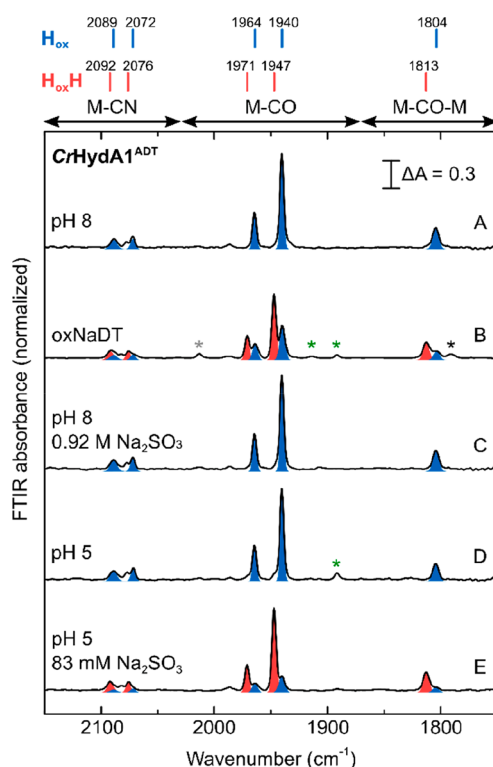

Figure 2. IR spectra of *Cr*HydA1[ADT] showing formation of $H_{ox}H$ with oxNaDT and Na_2SO_3 at low pH. IR spectra of *Cr*HydA1[ADT] were measured under a N_2 atmosphere at room temperature in 20 mM mixed buffer (see experimental section) pH 8 (A), in 0.83 M acidic oxNaDT (B), 0.92 M Na_2SO_3 pH 8 (C), in 20 mM mixed buffer pH 5 in the absence (D), or the presence (E) of 83 mM Na_2SO_3. Spectra were normalized to allow easier comparison from different measurements. Peaks for the H_{ox} and $H_{ox}H$ states are highlighted in blue and red, respectively. Small contributions from the H_{ox}-CO (gray asterisk), $H_{red}H^+$ (green), and H_{red} (black) states are indicated. Importantly, Na_2SO_3 solutions were pH corrected before use, whereas the solution of oxNaDT was not pH corrected, but measured to be around 2.

As shown by the IR spectra of *Cr*HydA1[ADT] (Figure 2), dilution of the enzyme in the oxNaDT solution results in the appearance of a new set of vibrational signals, slightly shifted to higher energy (<10 cm^{-1}) with respect to H_{ox}. These new signals are consistent with those reported for $H_{ox}H$.[10,19,27] Even though the pH of the oxNaDT solution was measured to be around 2, the buffer present in the *Cr*HydA1[ADT] sample (25 mM Tris-HCl, pH 8) will render the pH value after oxNaDT addition slightly higher than this (ca. pH 6). Interestingly, when *Cr*HydA1[ADT] was treated with a solution oxNaDT whose pH had been corrected to 7, conversion to $H_{ox}H$ was not observed (Figure S1), suggesting that formation of this state requires acidic conditions.

The observation that $H_{ox}H$ can be formed by treatment with oxidized NaDT challenges the hypothesis that $H_{ox}H$ and $H_{red}'H$ are protonated versions of the H-cluster. However, it was not clear which component of oxNaDT was interacting with the H-cluster. To better understand the nature of these two states and their role in the catalytic cycle of [FeFe] hydrogenases, we sought to identify the oxidation product(s) of NaDT responsible for their formation.

$H_{ox}H$ forms in the presence of sulfite at low pH. The main oxidation and degradation products of NaDT are sulfate
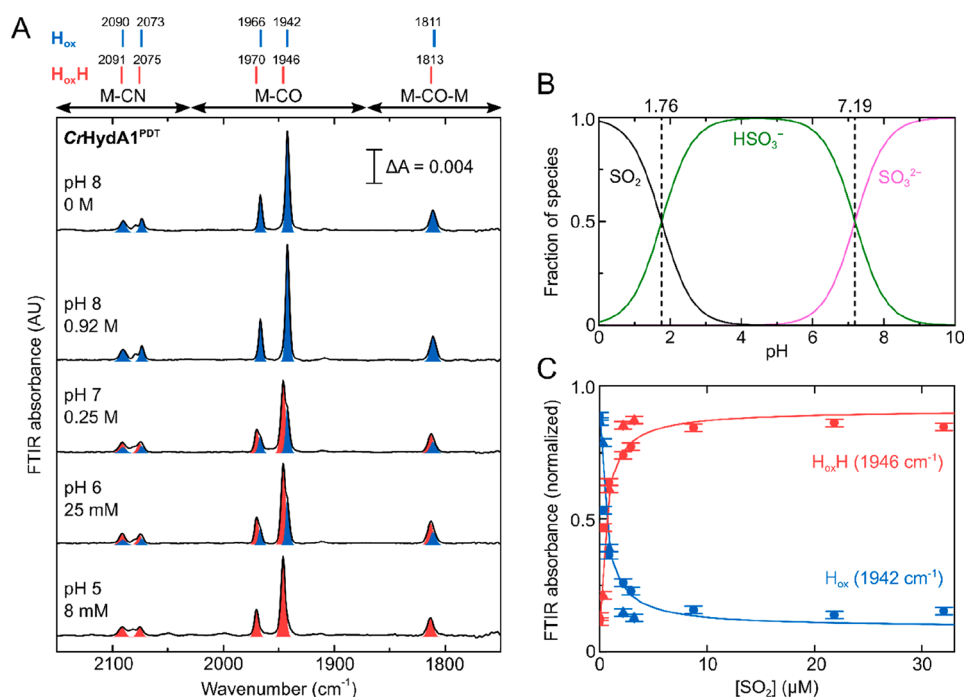
Figure 3. Titration of $CrHydA1^{PDT}$ with Na_2SO_3 under N_2 at various pH values. (A) IR spectra are shown for a range of conditions (pH 5−8) under various concentrations of Na_2SO_3 (0−0.92 M). The peaks for the H_{ox} and $H_{ox}H$ states are highlighted in blue and red, respectively. (B) Predicted speciation of sulfite in water as a function of the pH assuming an acid dissociation constant (pK_a) of 7.19 for $HSO_3^- \rightleftharpoons H^+ + SO_3^{2-}$ and an equilibrium constant (pK) of 1.76 for $SO_2 + H_2O \rightleftharpoons H^+ + HSO_3^-$.[50] (C) Variation in the intensity of the 1942 cm^{-1} (H_{ox}) and 1946 cm^{-1} ($H_{ox}H$) peaks with the estimated concentration of dissolved SO_2 at pH 7 (triangles) and 6 (circles). The data were fitted with a model describing binding of SO_2 to the hydrogenase with 1:1 stoichiometry and assuming that the concentration of SO_2 at equilibrium is determined only by the pH and the concentration of Na_2SO_3. The data at pH 6 and 7 were fitted simultaneously to the same model. For an expanded version of the region from 0 to 6 μM SO_2; see Figure S6E. Error bars (±standard deviation) were determined by measuring the 0, 0.25, and 0.92 M Na_2SO_3 spectra at pH 7 and the 25 mM Na_2SO_3 spectrum at pH 6 in triplicate, which gave standard deviations of less than 0.014.

(SO_4^{2-}), thiosulfate ($S_2O_3^{2-}$), and sulfite (SO_3^{2-}),[48,49] all of which could potentially interact with the H-cluster of $CrHydA1$ and cause conversion to the $H_{ox}H$ state. Therefore, to identify the NaDT oxidation products responsible for this conversion, we tested these species individually on $CrHydA1$ at both pH 8 and pH 5. Treatment of $CrHydA1$ with Na_2SO_4 and $Na_2S_2O_3$ at either pH 8 or pH 5 failed to reproduce the $H_{ox}H$ state (Figure S2). In contrast, we found that addition of 80 mM of Na_2SO_3 at pH 5 reproduced the effect of oxNaDT and caused almost full conversion to the $H_{ox}H$ state, while at pH 8 even a high concentration (0.92 M) of Na_2SO_3 had no effect on $CrHydA1$ (Figure 2). Importantly, $CrHydA1$ at pH 5 before addition of Na_2SO_3 has an identical spectrum to that at pH 8, demonstrating that both low pH and Na_2SO_3 are required for $H_{ox}H$ formation. Na_2SO_4, $Na_2S_2O_3$, and Na_2SO_3 solutions were pH corrected before use—this is particularly important for Na_2SO_3, which is a mild base.

In addition to $CrHydA1$, also the bacterial [FeFe] hydrogenases HydAB from *Desulfovibrio desulfuricans* (*Dd*HydAB) and HydA1 from *Clostridium pasteurianum* (*Cp*HydA1) have been reported to form the $H_{ox}H$ state at low pH and in the presence of NaDT.[27] These enzymes harbor additional [4Fe-4S] clusters (F-clusters) that form an electron-transfer chain from the protein surface to the H-cluster, and compared to $CrHydA1$, their active site is deeply buried inside the protein scaffold.[3,4] When treated with Na_2SO_3 under acidic conditions, also *Dd*HydAB and *Cp*HydA1 converted to the $H_{ox}H$ state (Figure S3), indicating that the interaction of the

H-cluster with the oxidation product of NaDT is a generalized phenomenon in [FeFe] hydrogenases.

A protonated form of sulfite interacts with the H-cluster. Next, we decided to carry out titrations of $CrHydA1$ with Na_2SO_3 at various pH values in order to provide further details on the particular form of Na_2SO_3 that binds, as well as determining the binding affinity. In order to simplify the titrations, we chose to use a chemical variant of $CrHydA1$ with a $[2Fe]_H$ analogue containing a propane dithiolate (PDT) bridging ligand instead of ADT (*Cr*HydA1^{PDT}, Figure 1A). Compared to the amine in ADT, the methylene group in PDT cannot be easily protonated. As a result, $CrHydA1^{PDT}$ has very low catalytic activity and the H-cluster cannot assume states with a reduced $[2Fe]_H$ (i.e., $H_{red}H^+$ and $H_{sred}H^+$) (Figure 1C). This greatly reduces the number of states observable in the IR spectra, simplifying data analysis. The PDT-containing enzyme was previously shown to convert to $H_{ox}H$ and $H_{red}'H$ at low pH in the presence of NaDT.[10,27] $CrHydA1^{PDT}$ was titrated with increasing amounts of Na_2SO_3 at five different pH values (Figure 3 and Figures S4−S6). In an anaerobic glovebox with a 100% N_2 atmosphere, the H-cluster was in the oxidized state H_{ox} at the beginning of the titration for all the pH values tested. As already observed for native $CrHydA1^{ADT}$, at pH 8 addition of even a very high concentration of Na_2SO_3 did not affect the state of the H-cluster, which remained in the H_{ox} state. Conversely, at pH 7, $H_{ox}H$ appeared already with less than 250 mM Na_2SO_3, and complete conversion was observed at around 700 mM. The concentration of Na_2SO_3 needed in order to observe complete
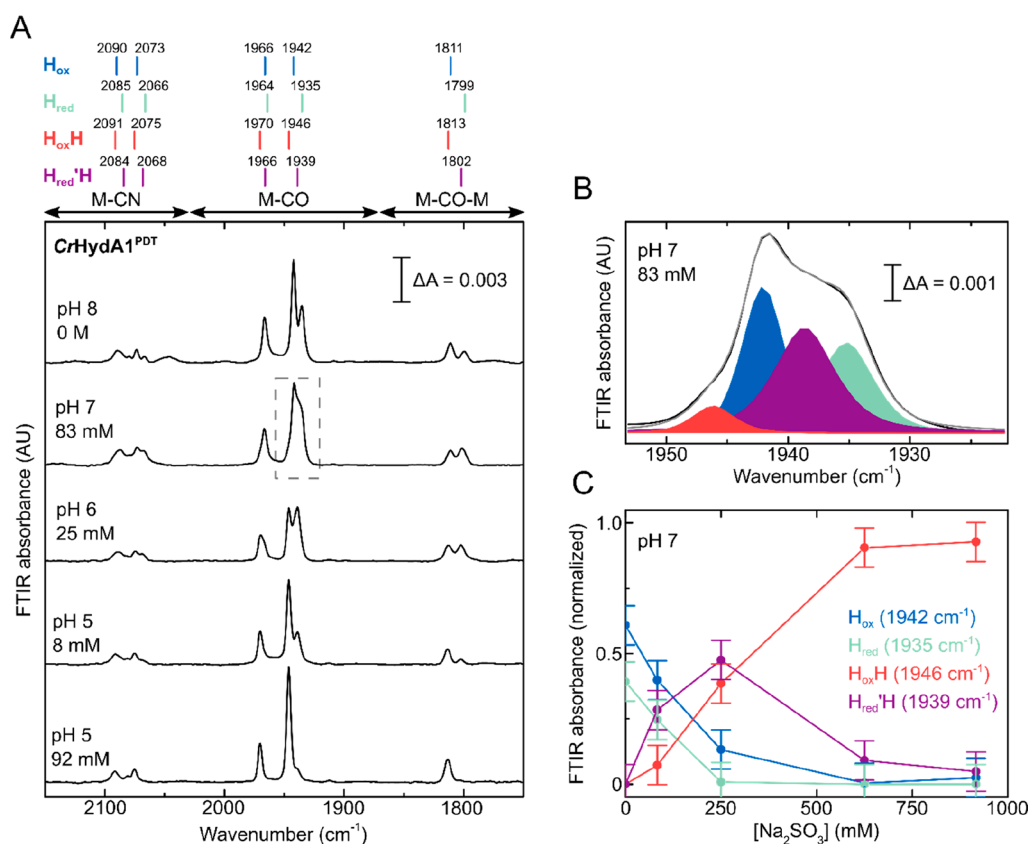
Figure 4. Titration of CrHydA1^{PDT} with Na$_2$SO$_3$ at various pH values under 2% H$_2$. (A) IR spectra are shown for a range of conditions (pH 5−8) under various concentrations of Na$_2$SO$_3$ (0−0.92 M). (B) Peak-fitting to pseudo-Voigt functions of the region between 1955 and 1920 cm^{-1} for the data in the dashed rectangle in A. Color code: H$_{ox}$ blue, H$_{red}$ cyan, H$_{ox}$H red, H$_{red}$'H purple. (C) The variation in the intensity of the 1942 cm^{-1} (H$_{ox}$), 1935 cm^{-1} (H$_{red}$), 1946 cm^{-1} (H$_{ox}$H), and 1939 cm^{-1} (H$_{red}$'H) peaks with the Na$_2$SO$_3$ concentration at pH 7. The lines connecting the points in C are for visual purposes only. Error bars (±standard deviation) were determined by measuring the 0, 0.25, and 0.92 M Na$_2$SO$_3$ spectra at pH 7 in triplicate, which gave standard deviations of less than 0.075.

conversion from H$_{ox}$ to H$_{ox}$H decreased at pH 6 to about 200 mM and at pH 5 to less than 8 mM. At pH 4, 1 mM Na$_2$SO$_3$ gave essentially complete conversion to H$_{ox}$H, while 1 mM Na$_2$SO$_3$ at pH 5 gave a roughly equal mixture of H$_{ox}$ and H$_{ox}$H (Figure S5).

In aqueous solutions SO$_3^{2-}$ is in equilibrium with its protonated form bisulfite (HSO$_3^-$), which in turn can be further protonated to form sulfurous acid (H$_2$SO$_3$), which immediately decomposes to sulfur dioxide (SO$_2$) and water (Figure 3B).[51−53] As Figure 3 shows, the lower the pH, the lower the concentration of sulfite needed to convert H$_{ox}$ to H$_{ox}$H. This, therefore, excludes that SO$_3^{2-}$, whose abundance is predicted to greatly decrease when changing the pH from 8 to 6, is responsible for formation of H$_{ox}$H. Since, as shown in Figure 3A, lowering the pH from 6 to 5, and then to 4 (Figure S5), caused a further reduction in the required concentration of Na$_2$SO$_3$ needed to convert H$_{ox}$ to H$_{ox}$H, while the fraction of HSO$_3^-$ should be constant in this range (Figure 3B), HSO$_3^-$ is also unlikely to be the form of Na$_2$SO$_3$ binding to the H-cluster. In a pH titration of Na$_2$SO$_3$ monitored by IR spectroscopy we observed that the intensity of peaks relative to HSO$_3^-$ indeed saturated after pH 6.0−5.5, while signals indicative of the presence of SO$_2$ appeared at pH 5 (Figure S7). Therefore, we hypothesize that the species interacting with the H-cluster to form H$_{ox}$H is SO$_2$. This seems reasonable considering that SO$_2$ is a neutral molecule able to easily diffuse through hydrophobic channels[54,55] to reach the H-cluster from

the protein surface, while the anions HSO$_3^-$ and SO$_3^{2-}$ will be prevented from entering due to their charge and their large hydration spheres in aqueous solution.[56] A similar suggestion was made to explain how S^{2-} reaches the H-cluster as H$_2$S to form the H$_{inact}$ state.[57]

At pH 7 and 6, even at high concentration of sulfite, the concentration of dissolved SO$_2$ is expected to be very low. Thus, in order to observe binding to the H-cluster and formation of H$_{ox}$H, SO$_2$ must have a tight affinity for the enzyme. Figure 3C shows the conversion from H$_{ox}$ to H$_{ox}$H as a function of the estimated concentration of SO$_2$ at each Na$_2$SO$_3$ addition, at either pH 6 or 7. The population of the two states was monitored from the intensity of the most prominent CO band at 1942 cm^{-1} for H$_{ox}$ and 1946 cm^{-1} for H$_{ox}$H, in both cases corresponding to the stretch of the terminal CO on Fe$_d$. The titration curves at pH 7 and 6 as a function of the concentration of SO$_2$ overlay nicely, in contrast to those obtained using the estimated concentrations of HSO$_3^-$ and SO$_3^{2-}$ (Figure S6). Fitting the data in Figure 3C to a simple equilibrium model describing one SO$_2$ molecule binding to the hydrogenase (SO$_2$ + E $\rightleftharpoons$ E:SO$_2$) gave an estimated binding affinity of ~500 nM. In our analysis, we considered that the pool of Na$_2$SO$_3$ can act as a buffer system for SO$_2$, replenishing what is consumed to form the enzyme:SO$_2$ complex (E:SO$_2$). For all the data points, the concentration of E:SO$_2$ formed was negligible compared to the total concentration of Na$_2$SO$_3$, so that the concentration of

SO_2 at equilibrium could be assumed to be independent of the formation of E:SO_2 and to be determined only by the pH and the total concentration of Na_2SO_3, an important consideration for such tight binding interactions. To put this in context, CO has been estimated to bind with 100 nM affinity to CrHydA1^{ADT}.[58]

Addition of sulfite under reducing conditions (H_2 atmosphere) forms $H_{red}'H$. The titration of CrHydA1^{PDT} with sulfite was repeated in the presence of 2% H_2 in the atmosphere of the anaerobic glovebox (Figure 4). Under these conditions, slow reactivity of the CrHydA1^{PDT} enzyme with H_2 can lead to reduction of the $[4Fe-4S]_H$ subcluster, in particular at high pH values. This is due to the potential of the $2H^+/H_2$ couple, which becomes more positive as the pH decreases, while the redox potential of $[4Fe-4S]_H$ is pH independent.[12] At pH 7, after addition of a small amount of Na_2SO_3, we observed a mixture of the H_{ox}, H_{red}, and $H_{ox}H$ states in the IR spectra, plus a new set of signals. These are consistent with the vibrational frequencies of the $H_{red}'H$ state, which Stripp and co-workers reported to form with NaDT at low pH and either under H_2 or at low electrochemical potential.[10,27] Similar to what was observed under N_2, at lower pH the formation of $H_{ox}H$ and $H_{red}'H$ was observed at lower concentration of Na_2SO_3. In order to estimate the proportion of each state present under each condition, we performed a pseudo-Voigt peak-fitting analysis of the region of the spectrum between $\sim$1955 cm^{-1} and $\sim$1920 cm^{-1}, containing the most dominant bands for H_{ox} (1942 cm^{-1}, blue), H_{red} (1935 cm^{-1}, cyan), $H_{ox}H$ (1946 cm^{-1}, red), and $H_{red}'H$ (1939 cm^{-1}, purple) (Figures 4B, S8–S10). In Figure 4C, the intensity of these contributions is plotted as a function of the concentration of Na_2SO_3 at pH 7. At low Na_2SO_3, both the $H_{ox}H$ and $H_{red}'H$ states are observed, but at high concentrations of Na_2SO_3 $H_{red}'H$ is converted to $H_{ox}H$. This indicates oxidation of the $[4Fe-4S]_H$ subcluster by Na_2SO_3. Since the samples were prepared in a closed IR cell and the concentrations of sulfite used are much higher than the dissolved concentration of H_2, oxidation by Na_2SO_3 will slowly deplete the H_2 concentration leading to oxidation of the sample. Similar behavior is observed also at pH 6 and 5 (Figures S8, S10).

At low concentrations (8 mM) of Na_2SO_3, at pH 6, the $H_{red}'H$ is the most dominant state, while $H_{ox}H$ becomes more favored at pH 5 at the same concentration of Na_2SO_3, agreeing with a pH independent redox potential of $[4Fe-4S]_H$ also when SO_2 is bound. However, the fact that SO_2 is more prevalent at low pH gives the conversion of H_{ox}/H_{red} to $H_{ox}H/H_{red}'H$ an "apparent" pH dependence. This will complicate the interpretation of pH-dependent redox titrations performed in the presence of oxidation products of sodium dithionite (including Na_2SO_3 and SO_2), which may explain discrepancies in the literature.[10,12]

Interestingly, at low concentrations of Na_2SO_3, the ratio of H_{ox}:H_{red} is much greater than that of $H_{ox}H$:$H_{red}'H$, suggesting that binding of SO_2 increases the redox potential of the $[4Fe-4S]_H$ subcluster (Figure 4B and S8, S9). The redox potential for the H_{ox}/H_{red} and $H_{ox}H/H_{red}'H$ transitions can be calculated at pH 6 and 7 at low concentrations of Na_2SO_3 from the populations of the four states (Figure S11). Using the Nernst equation, we found that E_m (H_{ox}/H_{red}) = -349 (±17) mV and E_m ($H_{ox}H/H_{red}'H$) = -293 (±26) mV. The value for E_m (H_{ox}/H_{red}) is in close agreement with that determined previously.[12,59] The fact that the redox potential for the $H_{ox}H/H_{red}'H$ transition is $\sim$60 mV more positive than the H_{ox}/H_{red}

transition also indicates a tighter binding affinity for SO_2 to the H_{red} state than to the H_{ox} state. We determined a K_d for SO_2 binding to the H_{ox} state of $\sim$500 nM from the titrations in the absence of H_2. By considering the thermodynamic cycle (Scheme 1) connecting the H_{ox}, H_{red}, $H_{ox}H$, and $H_{red}'H$ states,

Scheme 1. Thermodynamic Cycle Connecting H_{ox}, H_{red}, $H_{ox}H$, and $H_{red}'H$[a]
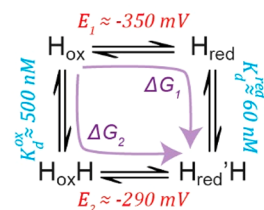
[a]One-electron reduction of H_{ox} and $H_{ox}H$ gives H_{red} and $H_{red}'H$, respectively, with redox potentials of $E_1 \approx -350$ mV and $E_2 \approx -290$ mV, respectively. H_{ox} and H_{red} convert to $H_{ox}H$ and $H_{red}'H$, respectively, by binding SO_2. The K_d for SO_2 binding to the H_{ox} state was measured to be $\sim$500 nM. By consideration of the fact that the Gibbs free energy is a state function, the ΔG associated with the transition from H_{ox} to $H_{red}'H$ is the same regardless of whether we go via H_{red} (ΔG_1) or via $H_{ox}H$ (ΔG_2), allowing us to calculate the K_d for binding of SO_2 to the H_{red} state to be $\sim$60 nM.

it can be calculated that an $\sim$60 mV difference in the redox potentials indicates a K_d of $\sim$60 nM for SO_2 binding to the H_{red} state, approximately 1 order of magnitude tighter. This also means that low concentrations of Na_2SO_3 have a larger effect in the presence of H_2 (compare Figure 4B with Figure S4B).

The site of SO_2 binding is not the open coordination site on $[2Fe]_H$. From the previous section, it is clear that SO_2 somehow interacts with the H-cluster of [FeFe] hydrogenases. It is tempting to speculate that SO_2 diffuses through the hydrophobic gas channel leading to the open coordination site on Fe_d. However, we cannot exclude that SO_2 binds elsewhere, and indeed, the change in the redox potential of $[4Fe-4S]_H$ would suggest that binding near to $[4Fe-4S]_H$ is more likely. To test whether binding of SO_2 with the H-cluster occurs at the open coordination site on $[2Fe]_H$, we investigated how its presence can affect the interaction of the enzyme with CO, a competitive inhibitor of [FeFe] hydrogenases that binds to Fe_d.[60] At pH 5 exposure of CrHydA1^{ADT} to 100% CO gas for 10 min in the absence of Na_2SO_3 generates pure H_{ox}-CO (Figure S12). In the presence of a high concentration of sulfite at pH 5, exposure of CrHydA1 to CO caused the appearance of new peaks that correspond to neither H_{ox}-CO nor $H_{ox}H$, and are similar to the $H_{ox}H$−CO state described by Stripp and co-workers (Figure S12).[27] This suggests that SO_2 does not compete for the same binding site as CO, which is the open coordination site at Fe_d.

In order to get further information on the SO_2 binding site, we measured ^{57}Fe nuclear resonance vibrational spectroscopy (NRVS). This technique measures Fe-ligand vibrational energies using nuclear excitation of ^{57}Fe and has been used extensively to probe ligand binding to the $[2Fe]_H$ subcluster in [FeFe] hydrogenase.[21−23,28,57] We artificially matured apo-CrHydA1 samples with a ^{57}Fe-labeled diiron subcluster precursor ($[2^{57}Fe]^{ADT}$) and measured NRVS in the H_{ox} and $H_{ox}H$ states (Figure 5). This enzyme is labeled with ^{57}Fe in the $[2Fe]_H$ subcluster and not in the $[4Fe-4S]_H$ subcluster, so only
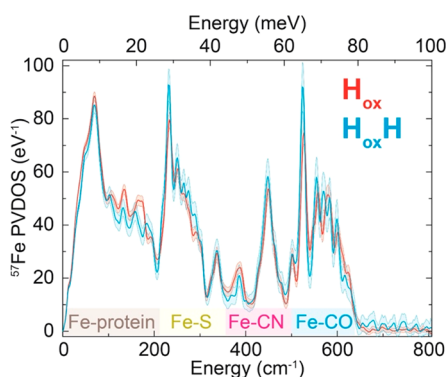
Figure 5. Comparison of the NRVS spectra of *Cr*HydA1 matured with an [57]Fe-labeled $[2Fe]^{ADT}$ precursor complex in the H_{ox} (red) and $H_{ox}H$ (blue) states measured at 10 K. The regions of the spectra corresponding to Fe-protein, Fe−S, Fe-CN, and Fe-CO vibrations are highlighted in brown, yellow, pink, and blue along the *x*-axis.

vibrations involving motion of the $[2Fe]_H$ subcluster can be observed. The spectra of H_{ox} and $H_{ox}H$ are very similar but with small shifts of the peaks to lower energy for the $H_{ox}H$, indicative of decreased electron density on the $[2Fe]_H$ subcluster, similar to results observed by Mebs *et al.*[28] In contrast, ligand binding to Fe_d on the $[2Fe]_H$ subcluster would be expected to have much more dramatic changes, particularly, the generation of additional Fe−S or Fe−O vibrations.[57,61] The results cannot definitively confirm the $[4Fe-4S]_H$ subcluster as the point of SO_2 binding, but together with the observation of the $H_{ox}H−CO$ state, they do exclude the open coordination site on Fe_d as the SO_2 binding site.

SO_2 inhibits catalysis by [FeFe] hydrogenase. In order to investigate the effect of SO_2-binding to the H-cluster on catalysis, we performed protein film electrochemistry on the *Dd*HydAB enzyme covalently attached to a pyrolytic graphite electrode. We chose *Dd*HydAB rather than *Cr*HydA1, as the former is, in our hands, much easier to covalently attach to graphite electrode surfaces.[62] As shown in the cyclic voltammograms (CVs) in Figure 6 and in the enlarged version of the CVs reported in Figure S13, a large negative current at low potentials is observed when Na_2SO_3 is injected into the electrochemical cell under acidic conditions (pH 5 and pH 6, respectively A and B in Figure 6). Controls experiments (bare graphite electrode injecting Na_2SO_3, Figure S14) suggest that this reduction current is likely due to HSO_3^- and SO_2 being reduced by the pyrolytic graphite electrode.[63] Comparisons of bare graphite electrodes and *Dd*HydAB-modified electrodes at various pH values are presented in the absence (Figure S15) and presence (Figure S16) of Na_2SO_3. Unfortunately, this massive reduction current masks the effect of Na_2SO_3 on the catalytic H^+-reduction current.

However, as shown in Figure 6A and B (CV at pH 5 and 6 in the presence of Na_2SO_3, respectively), in the presence of Na_2SO_3 the catalytic H_2-oxidation current decreases, suggesting inhibition of the enzyme as a result of the H-cluster somehow interacting with SO_2. The inhibitory effect on the catalytic H_2-oxidation current is more pronounced at lower pH (the CVs at pH 7 and 8 are reported in Figure 6C and D, respectively), in agreement with the pH-dependent formation of $H_{ox}H$ and $H_{red}'H$ observed in the IR measurements. To explore whether the inhibition is reversible and the electrocatalytic H_2-oxidation current can be recovered, the buffer in
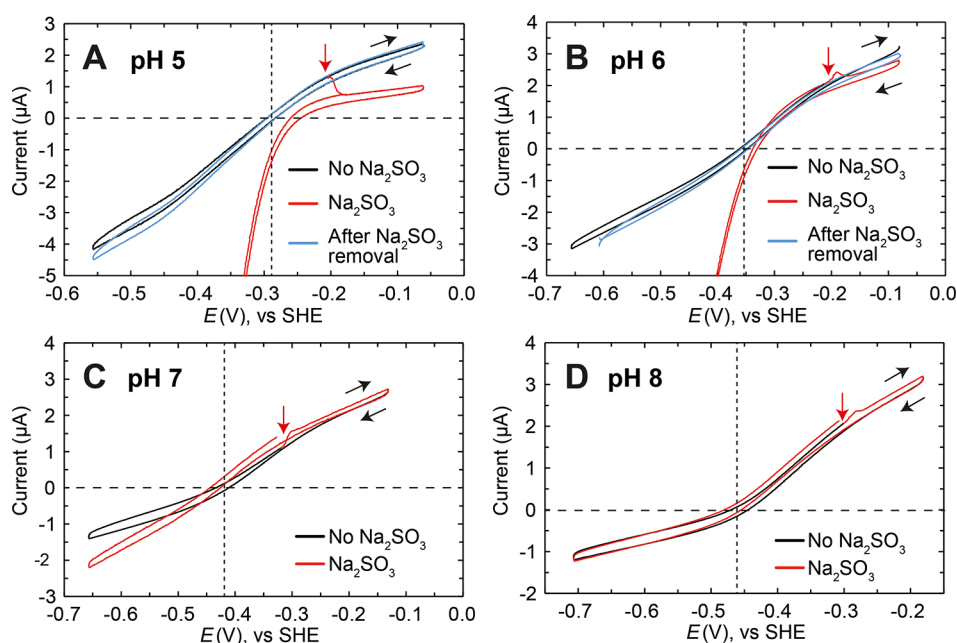

Figure 6. Protein film electrochemistry of *Dd*HydAB in the presence of sulfite. *Dd*HydAB was covalently attached to a pyrolytic graphite electrode and cyclic voltammetry (CV) was performed in 20 mM mixed buffer with 100 mM NaCl at pH 5 (A) 6 (B), 7 (C), and 8 (D) under 100% H_2 (1000 mL/min), at 25 °C, with 2000 rpm rotation, and a scan rate of 0.02 V/s. After 3 CVs in the absence of Na_2SO_3 (only the third trace is shown, black trace), 40 mM Na_2SO_3 was added (red trace). Only a single CV before and after the addition of Na_2SO_3 are shown. However, consecutive CVs showed the same shape. After replacing the buffer in the electrochemical cell with Na_2SO_3-free buffer, *Dd*HydAB recovered its original activity (blue traces). The red arrow indicates the point of Na_2SO_3 injection. The black arrows indicate the scan direction of the CV. The dashed horizontal line shows the zero current position, and the dashed vertical line shows the equilibrium $2H^+/H_2$ potential at each pH value. Enlarged versions of A and B are reported in Figure S13.
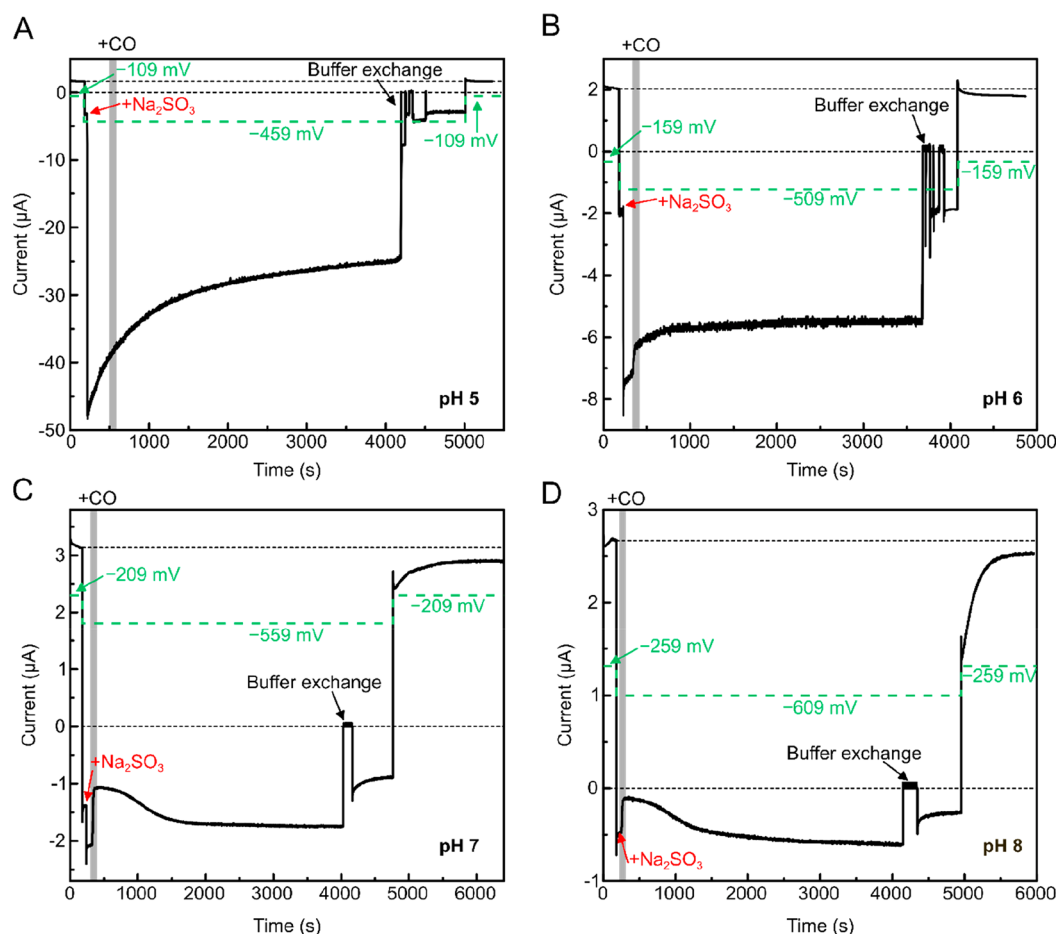
Figure 7. Chronoamperometry experiments of *Dd*HydAB in the presence of Na_2SO_3 and CO. Chronoamperometry experiments were performed on *Dd*HydAB covalently attached to a pyrolytic graphite electrode under 1 bar 90% H_2 in N_2 (1000 mL/min), in 20 mM mixed buffer with 100 mM NaCl at pH 5 (A), pH 6 (B), pH 7 (C), pH 8 (D) at 25 °C and 2000 rpm rotation rate. During the experiment the potential was sequentially stepped as indicated by the green profile (all potentials are reported *vs* SHE). For example, at pH 5 (A) the potential was initially set to −109 mV, next stepped down to −459 mV, and finally back to the initial potential −109 mV. Addition of 40 mM Na_2SO_3 is indicated by red arrows, while addition of 10% CO (in 90% H_2) to the gas mixture is indicated by the shaded gray area. After more than 3600 s, the buffer inside the electrochemical cell was rinsed and exchanged with fresh buffer without Na_2SO_3. Note the complex behavior in the region immediately following CO treatment at pH 6 in (B). This represents a convolution of the current recovery due to CO release and the exponential decay of the current as a result of decreasing Na_2SO_3 reduction. To observe the current recovery due to CO release, a simulated exponential decay curve was subtracted from the experimental data (Figure S17C), and the resulting difference curve is plotted in Figure S17D.

the electrochemical cell was exchanged to a fresh buffer without Na_2SO_3 during the course of the CVs. Sulfite-exposed *Dd*HydAB recovered 100% of the electrocatalytic H_2-oxidation current once Na_2SO_3 was removed from the electrochemical cell, suggesting that SO_2 binding and inhibition are fully reversible (blue trace in Figure 6A and B) and that the enzyme is not irreversibly damaged by SO_2.

The massive current at low potential due to direct reduction of HSO_3^- and SO_2 species by the electrode makes it difficult to assess the effect of Na_2SO_3 on the electrocatalytic H^+-reduction current. To distinguish the enzymatic contribution from the direct HSO_3^- and SO_2 reduction by the electrode, we performed chronoamperometry experiments (the applied potential is held at a specific value while the current is monitored *vs* time) in the presence and absence of CO (Figure 7). As previously described,[58,62] the current decrease due to CO addition (as CO binds to open coordination site on Fe_d and inhibits the enzyme) provides a direct measurement of the enzymatic H^+ reduction. In the experiment in Figure 7A, performed at pH 5, *Dd*HydAB attached on the pyrolytic

graphite electrode was initially exposed to 90% H_2/10% N_2 at −109 mV *vs* SHE, where a positive current due to H_2 oxidation was observed (as the applied potential is more positive than the thermodynamic potential of the $2H^+/H_2$ couple at this pH, −295 mV *vs* SHE). Switching to −459 mV gave a small negative current due to H^+ reduction (as the applied potential is now more negative than E_{2H^+/H_2} at this pH). Adding Na_2SO_3 at this potential gave an extremely large negative current, which was unaffected by addition of 10% CO into the gas feed (replacing the 10% N_2). This indicates that the large negative current is entirely due to Na_2SO_3 reduction and that catalytic H^+ reduction by *Dd*HydAB is completely inhibited under these conditions. Replacing the buffer with fresh Na_2SO_3-free buffer decreased the current to the original value observed before addition of Na_2SO_3. An analogous experiment at pH 6 (Figure 7B) showed a small decrease in the current after addition of CO, as well as experiments at pH 7 and pH 8 (Figure 7C and 7D, respectively), suggesting that at these pH values there is some contribution from the enzymatic H^+ reduction current, in agreement with the pH dependent formation of SO_2 from

Na_2SO_3. Control experiments in the complete absence of Na_2SO_3 showed full inhibition of the electrocatalytic H^+-reduction current by CO, thus demonstrating that in the absence of Na_2SO_3 the reductive current is indeed enzymatic H^+ reduction (Figure S17). At this stage, it is unclear whether the loss in activity in both directions due to Na_2SO_3 addition is directly related to the increase in the redox potential of $[4Fe-4S]_H$. The higher redox potential of the cluster may disrupt the proton-coupled electronic rearrangement between $[4Fe-4S]_H$ and $[2Fe]_H$.[14] These experiments help to understand the discrepancy between reported H^+ reduction activity solution assays and electrochemistry. While solution assays (where NaDT is used as electron source) indicate a maximum in activity at pH 7,[8] and almost no activity at pH 5, electrochemical measurements show the highest H^+ reduction activity at pH 5 (Figure S15). Regardless, these data show that, under the conditions where $H_{ox}H$ and $H_{red}'H$ form, the enzyme has lower activity, suggesting that these states are not active intermediates of the catalytic cycle of [FeFe] hydrogenases. This is in stark contrast to the suggestion from Stripp and Haumann that a catalytic cycle involving $H_{ox}H$ is actually the faster branch of the cycle compared to that involving the $H_{red}H^+$ and $H_{sred}H^+$ states (Figure 1D).

■ DISCUSSION

In this work we have shown that in *Cr*HydA1 the $H_{ox}H$ state forms in the presence of oxidation products of NaDT at low pH, specifically SO_2. SO_2 binding caused formation of $H_{ox}H$ not only with *Cr*HydA1 but also with the bacterial enzymes *Cp*HydA1 and *Dd*HydAB, suggesting this is a common behavior in [FeFe] hydrogenases. Additionally, we have shown that with Na_2SO_3 and in the presence of H_2 the reduced $H_{red}'H$ state can also form. The electrochemistry measurements showed loss in electrocatalytic activity when *Dd*HydAB was exposed to Na_2SO_3, especially at low pH, suggesting that $H_{ox}H$ and $H_{red}'H$ are less active states and challenging their inclusion in the catalytic cycle. Taken together, these findings suggest that $H_{ox}H$ and $H_{red}'H$ are not protonated versions of H_{ox} and H_{red}, but instead are forms of H_{ox} and H_{red} in which a product of NaDT oxidation, most likely SO_2, is bound. Thus, we suggest renaming $H_{ox}H$ and $H_{red}'H$ to $H_{ox}-DT_i$ and $H_{red}-DT_I$ (for dithionite inhibited) to avoid confusion, and for the rest of the discussion we will name them as such.

This result helps explain previous findings in the literature regarding these states. Originally, $H_{ox}-DT_i$ and $H_{red}-DT_i$ were discovered during NaDT-mediated H^+ reduction by [FeFe] hydrogenase at low pH.[19,27] Under these conditions H^+ reduction rates are high, leading to rapid oxidation of NaDT to generate a mixture of SO_3^{2-}, HSO_3^-, and SO_2. At low pH, SO_2 forms due to the protonation equilibria and it can bind to the hydrogenase yielding the $H_{ox}-DT_i$ and $H_{red}-DT_i$ states. It was noticed that the accumulation of $H_{ox}-DT_i$ was dependent both on pH and on NaDT concentration, both of which will affect the rate of SO_2 accumulation. Furthermore, it was noted that less active forms of the hydrogenase (e.g., with the PDT cofactor) accumulated $H_{ox}-DT_i$ more slowly. In this case, the accumulation of SO_2 depends on the rate of NaDT oxidation by the catalytic activity of the hydrogenase, and it is well established that the PDT-form of the hydrogenase is catalytically much less active than the native ADT-form.[64]

Protonation at $[4Fe-4S]_H$ is a critical component in the catalytic cycle proposed in Model 2 (Figure 1D). We recently demonstrated that (in the absence of NaDT) the redox potential of $[4Fe-4S]_H$ is pH-independent, challenging the involvement of PCET in the formation of H_{red} and the protonation at $[4Fe-4S]_H$.[12] Our current work further challenges protonation at $[4Fe-4S]_H$ by showing that the Model 2 key intermediate $H_{ox}-DT_i$ ($H_{ox}H$ in Figure 1D) is generated by the oxidation products of NaDT. If reduction of $[4Fe-4S]_H$ is coupled to protonation then it has to be coupled to protonation in all the steps involving reduction of $[4Fe-4S]_H$. Considering that the hydrogenase enzyme is reversible, with a very low overpotential in either direction, it must be assumed that each step in the catalytic cycle is also reversible and, thus, H_{ox} should be able to protonate to give $H_{ox}-DT_i$. However, incubation of H_{ox} at low pH in the absence of NaDT does not generate $H_{ox}-DT_i$ (Figure 2), so $H_{ox}-DT_i$ is clearly not a reversibly protonated form of H_{ox}.

Our results also help to explain the misassignment of the pH dependence of the H_{ox}/H_{red} transition. It is important to recall that in this study we also observe that the $H_{ox}-DT_i/H_{red}-DT_i$ transition is about 60 mV more positive than the H_{ox}/H_{red} transition, as also reported by Senger et al.[10] If the conversion of H_{ox} to $H_{ox}-DT_i$ and H_{red} to $H_{red}-DT_i$ depend on the pH, then we expect that the "apparent" redox potential of both transitions will shift from the intrinsic redox potential of H_{ox}/H_{red} to the intrinsic redox potential of $H_{ox}-DT_i/H_{red}-DT_i$ as the pH is decreased. This is simply a consequence of the redox and protonation equilibria being coupled (see Supporting Information and Figure S18 for further details and a model illustrating this behavior). As we demonstrated that the SO_2 concentration in solution increases with decreasing pH and that SO_2 is responsible for binding to H_{ox}/H_{red} to generate $H_{ox}-DT_i/H_{red}-DT_i$, then this gives us a pH dependent conversion of H_{ox}/H_{red} to $H_{ox}-DT_i/H_{red}-DT_i$ and, therefore, an apparent pH dependence of the redox potential.

A further important finding regarding the [FeFe] hydrogenase is the fact that SO_2 appears to inhibit the H_2 oxidation and H^+ reduction activity of the enzyme. This may be due to the increased redox potential of $[4Fe-4S]_H$. While we do not yet completely understand this effect, it highlights the importance of the balance of redox potentials between the two parts of the H-cluster in facilitating electronic coupling and efficient catalysis. We previously showed that mutation of a cysteine ligating $[4Fe-4S]_H$ to histidine increased the redox potential by ∼200 mV. This completely abolished H^+ reduction activity, while actually enhancing H_2 oxidation at high overpotentials.[65]

The now well-characterized H_{hyd} intermediate can be generated under conditions of high NaDT at low pH. It is not clear yet whether this state is also somehow influenced by the presence of SO_2. However, it has always been intriguing how such an intermediate could be so stable by simply generating it at low pH in the presence of NaDT. Previous explanations have employed Le Chatelier's principle and the concept of proton pressure.[19] It may indeed be the case that SO_2 binding stabilizes the H_{hyd} state by increasing the redox potential of the $[4Fe-4S]_H$ subcluster slowing electron transfer to $[2Fe]_H$ to generate H_2. Recent evidence shows that versions of H_{hyd} can be generated from $H_{red}H^+$ and $H_{sred}H^+$.[25] The so-called $H_{hyd:red}$ state is generated from $H_{sred}H^+$ and should have a reduced $[4Fe-4S]_H$ subcluster analogous to H_{hyd}. Interestingly, the IR bands of H_{hyd} are shifted to higher energy compared with $H_{hyd:red}$ by a similar amount to $H_{ox}-DT_i$ *vs* H_{ox} (Table S2). Careful revaluation of the H_{hyd} state generated with NaDT at low pH is clearly necessary.

In addition to shedding light on the catalytic cycle of [FeFe] hydrogenases, this work reports how NaDT, a compound commonly employed as a reducing agent in metalloenzyme research, is responsible for the generation of artifacts, which were erroneously characterized as catalytically relevant states. To our knowledge, this is the first report of such "non-innocent" behavior of NaDT with [FeFe] hydrogenases, in this case caused by the interaction of one of the NaDT oxidation products with the enzyme. The experimental conditions should, thus, be carefully evaluated when NaDT is chosen as the reducing agent with these enzymes. As we have shown, acidic conditions facilitate formation of H_{ox}-DT_i, but at a high concentration of sulfite this state also forms at pH 7. Therefore, particular care must be taken when [FeFe] hydrogenase samples that contain (or contained) NaDT are studied at low pH, or in those cases where NaDT is used as a continuous source of electrons. While this is the first time that NaDT has been shown to interfere with spectroscopic studies of [FeFe] hydrogenases, several previous studies of various other metalloenzymes have reported similar effects. This problematic behavior has been attributed to several factors, from the slow kinetics of NaDT dissociation limiting the catalytic behavior to the unwanted interaction of its oxidation products with the system under study, as we described for [FeFe] hydrogenases. Importantly, the enzymes affected catalyze various reactions and harbor various metallocofactors, suggesting that it is difficult to predict which enzymes will be affected. As such, it is possible that similar effects are still going undetected for other systems. Therefore, the chemistry of NaDT and of its oxidation products should be carefully considered when choosing this compound as a reducing agent for metalloproteins research, and important control experiments should be routinely employed to identify possible side-reactions that can engage with the system under study. In the future it will also be important to evaluate alternative artificial reductants such as Ti(III) citrate ($E^{0'} < -800$ mV vs SHE[66]) and Eu(II)-DPTA ($E^{0'} < -1$ V vs SHE[67]) or the physiological redox partners for their use in hydrogenase research as well as with other metalloproteins.

Inhibition of [FeFe] hydrogenases by sulfite may not simply be an artifact but could represent a physiological mechanism for diverting electrons away from H^+ reduction by hydrogenase and toward sulfite reduction by dissimilatory and assimilatory sulfite reductases. Here, we showed that the [FeFe] hydrogenases from *C. reinhardtii*, *D. desulfuricans*, and *C. pasteurianum* all form the $H_{ox}H$ state in the presence of sulfite, each of which contains a sulfite reductase. In *C. reinhardtii* and *C. pasteurianum*, both [FeFe] hydrogenase and sulfite reductase receive electrons from ferredoxin.[68−70] Inhibition of the hydrogenase by sulfite would divert electrons from H^+ reduction to sulfite reduction. In *D. desulfuricans*, [FeFe] hydrogenase supplies electrons for sulfite reduction via a membrane bound electron transport chain,[71] and so inhibition of H_2 oxidation could stop electron transfer to the sulfite reductase, increasing sulfite concentrations even further. However, under conditions of high H_2S, the sulfite reductase is reversed, producing sulfite from H_2S, leading to reverse electron transport and H^+ reduction by [FeFe] hydrogenase. Inhibition of H^+ reduction by sulfite would prevent this H_2S oxidation and stop sulfite accumulation.

CONCLUSIONS

In this work we have shown that SO_2, an oxidation product of the commonly used nonphysiological reductant sodium dithionite, binds tightly to [FeFe] hydrogenase converting the catalytic intermediate states H_{ox} and H_{red} into the H_{ox}-DT_i and H_{red}-DT_i states (previously named $H_{ox}H$ and $H_{red}H$). Thus, our results do not support the notion of protonation of the $[4Fe-4S]_H$ subcluster of the H-cluster, nor that the H_{ox}-DT_i state is a critical intermediate in the catalytic cycle. SO_2 most likely binds at or near the $[4Fe-4S]$ subcluster and appears to increase the cluster redox potential. This in turn may explain the observed decrease in catalytic activity. Overall, these results highlight the importance of finely tuned redox potentials for catalytic activity and reversibility. More generally, these results should come as a cautionary note to all who use sodium dithionite in metalloprotein studies without concern for its "non-innocent" effects. Sodium dithionite is routinely used in studies on a wide range of metalloenzymes including nitrogenase, CO dehydrogenase, formate dehydrogenase, and many more. Careful evaluation of results from a range of nonphysiological reductants should help to establish the effects that are artifacts from those that represent the physiological behavior of the enzyme of interest.

ASSOCIATED CONTENT

Supporting Information

The Supporting Information is available free of charge at https://pubs.acs.org/doi/10.1021/jacs.1c07322.

Experimental section, supplementary figures and tables, supplementary discussion (PDF)

AUTHOR INFORMATION

Corresponding Authors

James A. Birrell − *Department of Inorganic Spectroscopy, Max Planck Institute for Chemical Energy Conversion, 45470 Mülheim an der Ruhr, Germany;* orcid.org/0000-0002-0939-0573; Email: james.birrell@cec.mpg.de

Patricia Rodríguez-Maciá − *Inorganic Chemistry Laboratory, Department of Chemistry, University of Oxford, Oxford OX1 3QR, U.K.;* orcid.org/0000-0003-3513-0115; Email: patricia.rodriguezmacia@chem.ox.ac.uk

Authors

Maria Alessandra Martini − *Department of Inorganic Spectroscopy, Max Planck Institute for Chemical Energy Conversion, 45470 Mülheim an der Ruhr, Germany*

Olaf Rüdiger − *Department of Inorganic Spectroscopy, Max Planck Institute for Chemical Energy Conversion, 45470 Mülheim an der Ruhr, Germany;* orcid.org/0000-0002-5148-9083

Nina Breuer − *Department of Inorganic Spectroscopy, Max Planck Institute for Chemical Energy Conversion, 45470 Mülheim an der Ruhr, Germany*

Birgit Nöring − *Department of Inorganic Spectroscopy, Max Planck Institute for Chemical Energy Conversion, 45470 Mülheim an der Ruhr, Germany*

Serena DeBeer − *Department of Inorganic Spectroscopy, Max Planck Institute for Chemical Energy Conversion, 45470 Mülheim an der Ruhr, Germany;* orcid.org/0000-0002-5196-3400

Complete contact information is available at:
https://pubs.acs.org/10.1021/jacs.1c07322

■ **REFERENCES**

(1) Lubitz, W.; Ogata, H.; Rüdiger, O.; Reijerse, E. Hydrogenases. *Chem. Rev.* **2014**, *114* (8), 4081−148.

(2) Land, H.; Senger, M.; Berggren, G.; Stripp, S. T. Current state of [FeFe]-hydrogenase research: biodiversity and spectroscopic investigations. *ACS Catal.* **2020**, *10* (13), 7069−7086.

(3) Peters, J. W.; Lanzilotta, W. N.; Lemon, B. J.; Seefeldt, L. C. X-ray crystal structure of the Fe-only hydrogenase (*Cp*I) from *Clostridium pasteurianum* to 1.8 angstrom resolution. *Science* **1998**, *282* (5395), 1853.

(4) Nicolet, Y.; Piras, C.; Legrand, P.; Hatchikian, C. E.; Fontecilla-Camps, J. C. *Desulfovibrio desulfuricans* iron hydrogenase: the structure shows unusual coordination to an active site Fe binuclear center. *Structure* **1999**, *7* (1), 13−23.

(5) Silakov, A.; Wenk, B.; Reijerse, E.; Lubitz, W. ^{14}N HYSCORE investigation of the H-cluster of [FeFe] hydrogenase: evidence for a nitrogen in the dithiol bridge. *Phys. Chem. Chem. Phys.* **2009**, *11* (31), 6592−6599.

(6) Berggren, G.; Adamska, A.; Lambertz, C.; Simmons, T. R.; Esselborn, J.; Atta, M.; Gambarelli, S.; Mouesca, J. M.; Reijerse, E.; Lubitz, W.; Happe, T.; Artero, V.; Fontecave, M. Biomimetic assembly and activation of [FeFe]-hydrogenases. *Nature* **2013**, *499* (7456), 66−69.

(7) Roseboom, W.; De Lacey, A. L.; Fernandez, V. M.; Hatchikian, E. C.; Albracht, S. P. J. The active site of the [FeFe]-hydrogenase from *Desulfovibrio desulfuricans*. II. Redox properties, light sensitivity and CO-ligand exchange as observed by infrared spectroscopy. *JBIC, J. Biol. Inorg. Chem.* **2006**, *11* (1), 102−118.

(8) Haumann, M.; Stripp, S. T. The molecular proceedings of biological hydrogen turnover. *Acc. Chem. Res.* **2018**, *51* (8), 1755−1763.

(9) Sanchez, M. L. K.; Sommer, C.; Reijerse, E.; Birrell, J. A.; Lubitz, W.; Dyer, R. B. Investigating the kinetic competency of *Cr*HydA1 [FeFe] hydrogenase intermediate states via time-resolved infrared spectroscopy. *J. Am. Chem. Soc.* **2019**, *141* (40), 16064−16070.

(10) Senger, M.; Laun, K.; Wittkamp, F.; Duan, J.; Haumann, M.; Happe, T.; Winkler, M.; Apfel, U. P.; Stripp, S. T. Proton-coupled reduction of the catalytic [4Fe-4S] cluster in [FeFe]-hydrogenases. *Angew. Chem., Int. Ed.* **2017**, *56* (52), 16503−16506.

(11) Ratzloff, M. W.; Artz, J. H.; Mulder, D. W.; Collins, R. T.; Furtak, T. E.; King, P. W. CO-bridged H-cluster intermediates in the catalytic mechanism of [FeFe]-hydrogenase *Ca*I. *J. Am. Chem. Soc.* **2018**, *140* (24), 7623−7628.

(12) Rodríguez-Maciá, P.; Breuer, N.; DeBeer, S.; Birrell, J. A. Insight into the redox behavior of the [4Fe-4S] subcluster in [FeFe] hydrogenases. *ACS Catal.* **2020**, *10* (21), 13084−13095.

(13) Reijerse, E. J.; Pelmenschikov, V.; Birrell, J. A.; Richers, C. P.; Kaupp, M.; Rauchfuss, T. B.; Cramer, S. P.; Lubitz, W. Asymmetry in the ligand coordination sphere of the [FeFe] hydrogenase active site is reflected in the magnetic spin interactions of the aza-propanedithiolate ligand. *J. Phys. Chem. Lett.* **2019**, *10* (21), 6794−6799.

(14) Sommer, C.; Adamska-Venkatesh, A.; Pawlak, K.; Birrell, J. A.; Rüdiger, O.; Reijerse, E. J.; Lubitz, W. Proton coupled electronic rearrangement within the H-cluster as an essential step in the catalytic cycle of [FeFe] hydrogenases. *J. Am. Chem. Soc.* **2017**, *139* (4), 1440−1443.

(15) Katz, S.; Noth, J.; Horch, M.; Shafaat, H. S.; Happe, T.; Hildebrandt, P.; Zebger, I. Vibrational spectroscopy reveals the initial steps of biological hydrogen evolution. *Chem. Sci.* **2016**, *7* (11), 6746−6752.

(16) Adamska, A.; Silakov, A.; Lambertz, C.; Rüdiger, O.; Happe, T.; Reijerse, E.; Lubitz, W. Identification and characterization of the "super-reduced" state of the H-cluster in [FeFe] hydrogenase: a new building block for the catalytic cycle? *Angew. Chem., Int. Ed.* **2012**, *51* (46), 11458−11462.

(17) Silakov, A.; Kamp, C.; Reijerse, E.; Happe, T.; Lubitz, W. Spectroelectrochemical characterization of the active site of the [FeFe] hydrogenase HydA1 from *Chlamydomonas reinhardtii*. *Biochemistry* **2009**, *48* (33), 7780−7786.

(18) Mulder, D. W.; Ratzloff, M. W.; Bruschi, M.; Greco, C.; Koonce, E.; Peters, J. W.; King, P. W. Investigations on the role of proton-coupled electron transfer in hydrogen activation by [FeFe]-hydrogenase. *J. Am. Chem. Soc.* **2014**, *136* (43), 15394−15402.

(19) Winkler, M.; Senger, M.; Duan, J.; Esselborn, J.; Wittkamp, F.; Hofmann, E.; Apfel, U.-P.; Stripp, S. T.; Happe, T. Accumulating the hydride state in the catalytic cycle of [FeFe]-hydrogenases. *Nat. Commun.* **2017**, *8* (1), 16115.

(20) Mulder, D. W.; Guo, Y.; Ratzloff, M. W.; King, P. W. Identification of a catalytic iron-hydride at the H-cluster of [FeFe]-hydrogenase. *J. Am. Chem. Soc.* **2017**, *139* (1), 83−86.

(21) Pelmenschikov, V.; Birrell, J. A.; Pham, C. C.; Mishra, N.; Wang, H.; Sommer, C.; Reijerse, E.; Richers, C. P.; Tamasaku, K.; Yoda, Y.; Rauchfuss, T. B.; Lubitz, W.; Cramer, S. P. Reaction coordinate leading to H₂ production in [FeFe]-hydrogenase identified by nuclear resonance vibrational spectroscopy and density functional theory. *J. Am. Chem. Soc.* **2017**, *139* (46), 16894−16902.

(22) Pham, C. C.; Mulder, D. W.; Pelmenschikov, V.; King, P. W.; Ratzloff, M. W.; Wang, H.; Mishra, N.; Alp, E. E.; Zhao, J.; Hu, M. Y.; Tamasaku, K.; Yoda, Y.; Cramer, S. P. Terminal hydride species in [FeFe]-hydrogenases are vibrationally coupled to the active site environment. *Angew. Chem., Int. Ed.* **2018**, *57* (33), 10605−10609.

(23) Reijerse, E. J.; Pham, C. C.; Pelmenschikov, V.; Gilbert-Wilson, R.; Adamska-Venkatesh, A.; Siebel, J. F.; Gee, L. B.; Yoda, Y.; Tamasaku, K.; Lubitz, W.; Rauchfuss, T. B.; Cramer, S. P. Direct observation of an iron-bound terminal hydride in [FeFe]-hydrogenase by nuclear resonance vibrational spectroscopy. *J. Am. Chem. Soc.* **2017**, *139* (12), 4306−4309.

(24) Lautier, T.; Ezanno, P.; Baffert, C.; Fourmond, V.; Cournac, L.; Fontecilla-Camps, J. C.; Soucaille, P.; Bertrand, P.; Meynial-Salles, I.; Léger, C. The quest for a functional substrate access tunnel in FeFe hydrogenase. *Faraday Discuss.* **2011**, *148* (0), 385−407.

(25) Lorent, C.; Katz, S.; Duan, J.; Kulka, C. J.; Caserta, G.; Teutloff, C.; Yadav, S.; Apfel, U.-P.; Winkler, M.; Happe, T.; Horch, M.; Zebger, I. Shedding light on proton and electron dynamics in [FeFe] hydrogenases. *J. Am. Chem. Soc.* **2020**, *142* (12), 5493−5497.

(26) Esselborn, J.; Muraki, N.; Klein, K.; Engelbrecht, V.; Metzler-Nolte, N.; Apfel, U. P.; Hofmann, E.; Kurisu, G.; Happe, T. A

structural view of synthetic cofactor integration into [FeFe]-hydrogenases. *Chem. Sci.* **2016**, *7* (2), 959−968.

(27) Senger, M.; Mebs, S.; Duan, J.; Shulenina, O.; Laun, K.; Kertess, L.; Wittkamp, F.; Apfel, U. P.; Happe, T.; Winkler, M.; Haumann, M.; Stripp, S. T. Protonation/reduction dynamics at the [4Fe-4S] cluster of the hydrogen-forming cofactor in [FeFe]-hydrogenases. *Phys. Chem. Chem. Phys.* **2018**, *20* (5), 3128−3140.

(28) Mebs, S.; Duan, J.; Wittkamp, F.; Stripp, S. T.; Happe, T.; Apfel, U.-P.; Winkler, M.; Haumann, M. Differential protonation at the catalytic six-iron cofactor of [FeFe]-hydrogenases revealed by ^{57}Fe nuclear resonance X-ray scattering and quantum mechanics/molecular mechanics analyses. *Inorg. Chem.* **2019**, *58* (6), 4000−4013.

(29) Mayhew, S. G. The redox potential of dithionite and SO_2^- from equilibrium reactions with flavodoxins, methyl viologen and hydrogen plus hydrogenase. *Eur. J. Biochem.* **1978**, *85* (2), 535−547.

(30) Mirts, E. N.; Petrik, I. D.; Hosseinzadeh, P.; Nilges, M. J.; Lu, Y. A designed heme-[4Fe-4S] metalloenzyme catalyzes sulfite reduction like the native enzyme. *Science* **2018**, *361* (6407), 1098−1101.

(31) Schnell, R.; Sandalova, T.; Hellman, U.; Lindqvist, Y.; Schneider, G. Siroheme- and [Fe4-S4]-dependent NirA from *Mycobacterium tuberculosis* is a sulfite reductase with a covalent Cys-Tyr bond in the active site. *J. Biol. Chem.* **2005**, *280* (29), 27319−28.

(32) Siegel, L. M.; Murphy, M. J.; Kamin, H. Reduced nicotinamide adenine dinucleotide phosphate-sulfite reductase of enterobacteria. *J. Biol. Chem.* **1973**, *248* (1), 251−264.

(33) Tanifuji, K.; Lee, C. C.; Sickerman, N. S.; Tatsumi, K.; Ohki, Y.; Hu, Y.; Ribbe, M. W. Tracing the 'ninth sulfur' of the nitrogenase cofactor via a semi-synthetic approach. *Nat. Chem.* **2018**, *10* (5), 568−572.

(34) Blackmore, R. S.; Gadsby, P. M. A.; Greenwood, C.; Thomson, A. J. Spectroscopic studies of partially reduced forms of *Wolinella succinogenes* nitrite reductase. *FEBS Lett.* **1990**, *264* (2), 257−262.

(35) Costa, C.; Moura, J. J. G.; Moura, I.; Wang, Y.; Huynh, B. H. Redox properties of cytochrome c nitrite reductase from *Desulfovibrio desulfuricans* ATCC 27774. *J. Biol. Chem.* **1996**, *271* (38), 23191−23196.

(36) Vega, J. M.; Kamin, H. Spinach nitrite reductase. Purification and properties of a siroheme-containing iron-sulfur enzyme. *J. Biol. Chem.* **1977**, *252* (3), 896−909.

(37) McAlpine, A. S.; McEwan, A. G.; Shaw, A. L.; Bailey, S. Molybdenum active centre of DMSO reductase from *Rhodobacter capsulatus*: crystal structure of the oxidised enzyme at 1.82-Å resolution and the dithionite-reduced enzyme at 2.8-Å resolution. *JBIC, J. Biol. Inorg. Chem.* **1997**, *2* (6), 690−701.

(38) Hao, B.; Zhao, G.; Kang, P. T.; Soares, J. A.; Ferguson, T. K.; Gallucci, J.; Krzycki, J. A.; Chan, M. K. Reactivity and chemical synthesis of L-pyrrolysine- the 22nd genetically encoded amino acid. *Chem. Biol.* **2004**, *11* (9), 1317−24.

(39) Russell, W. K.; Stålhandske, C. M. V.; Xia, J.; Scott, R. A.; Lindahl, P. A. Spectroscopic, redox, and structural characterization of the Ni-labile and nonlabile forms of the acetyl-CoA synthase active site of carbon monoxide dehydrogenase. *J. Am. Chem. Soc.* **1998**, *120* (30), 7502−7510.

(40) Golden, E.; Karton, A.; Vrielink, A. High-resolution structures of cholesterol oxidase in the reduced state provide insights into redox stabilization. *Acta Crystallogr., Sect. D: Biol. Crystallogr.* **2014**, *70* (12), 3155−66.

(41) Mager, H. I.; Tu, S. C. Dithionite treatment of flavins: spectral evidence for covalent adduct formation and effect on in vitro bacterial bioluminescence. *Photochem. Photobiol.* **1990**, *51* (2), 223−9.

(42) Marshall, S. A.; Fisher, K.; Ni Cheallaigh, A.; White, M. D.; Payne, K. A.; Parker, D. A.; Rigby, S. E.; Leys, D. Oxidative maturation and structural characterization of prenylated FMN binding by UbiD, a decarboxylase involved in bacterial ubiquinone biosynthesis. *J. Biol. Chem.* **2017**, *292* (11), 4623−4637.

(43) Dolphin, D. H.; Johnson, A. W.; Shaw, N. Sulphitocobalamin. *Nature* **1963**, *199* (4889), 170−171.

(44) Salnikov, D. S.; Silaghi-Dumitrescu, R.; Makarov, S. V.; van Eldik, R.; Boss, G. R. Cobalamin reduction by dithionite. Evidence for

the formation of a six-coordinate cobalamin(II) complex. *Dalton Trans.* **2011**, *40* (38), 9831−4.

(45) Yang, Z.-Y.; Ledbetter, R.; Shaw, S.; Pence, N.; Tokmina-Lukaszewska, M.; Eilers, B.; Guo, Q.; Pokhrel, N.; Cash, V. L.; Dean, D. R.; Antony, E.; Bothner, B.; Peters, J. W.; Seefeldt, L. C. Evidence that the Pi release event is the rate-limiting step in the nitrogenase catalytic cycle. *Biochemistry* **2016**, *55* (26), 3625−3635.

(46) Spencer, M. S. Chemistry of sodium dithionite. Part 1.—Kinetics of decomposition in aqueous bisulphite solutions. *Trans. Faraday Soc.* **1967**, *63* (0), 2510−2515.

(47) Wayman, M.; Lem, W. J. Decomposition of aqueous dithionite. Part II. A reaction mechanism for the decomposition of aqueous sodium dithionite. *Can. J. Chem.* **1970**, *48* (5), 782−787.

(48) Meyer, J. Zur Kenntnis der hydroschwefligen Säure. *Z. Anorg. Allg. Chem.* **1903**, *34* (1), 43−61.

(49) Rinker, R. G.; Gordon, T. P.; Mason, D. M.; Sakaida, R. R.; Corcoran, W. H. Kinetics and mechanism of the air oxidation of the dithionite ion ($S_2O_4^{2-}$) in aqueous solution. *J. Phys. Chem.* **1960**, *64* (5), 573−581.

(50) Selwyn, L.; Tse, S. The chemistry of sodium dithionite and its use in conservation. *Stud. Conserv.* **2008**, *53* (sup2), 61−73.

(51) Bishenden, E.; Donaldson, D. J. Ab initio study of SO_2 + H_2O. *J. Phys. Chem. A* **1998**, *102* (24), 4638−4642.

(52) Sinha, R. K.; Scuderi, D.; Maitre, P.; Chiavarino, B.; Crestoni, M. E.; Fornarini, S. Elusive sulfurous acid: gas-phase basicity and IR signature of the protonated species. *J. Phys. Chem. Lett.* **2015**, *6* (9), 1605−1610.

(53) Voegele, A. F.; Tautermann, C. S.; Loerting, T.; Hallbrucker, A.; Mayer, E.; Liedl, K. R. About the stability of sulfurous acid (H_2SO_3) and its dimer. *Chem. - Eur. J.* **2002**, *8* (24), 5644−5651.

(54) Nicolet, Y.; Lemon, B. J.; Fontecilla-Camps, J. C.; Peters, J. W. A novel FeS cluster in Fe-only hydrogenases. *Trends Biochem. Sci.* **2000**, *25* (3), 138−143.

(55) Cohen, J.; Kim, K.; King, P.; Seibert, M.; Schulten, K. Finding gas diffusion pathways in proteins: application to O_2 and H_2 transport in *Cp*I [FeFe]-hydrogenase and the role of packing defects. *Structure* **2005**, *13* (9), 1321−1329.

(56) Eklund, L.; Hofer, T. S.; Pribil, A. B.; Rode, B. M.; Persson, I. On the structure and dynamics of the hydrated sulfite ion in aqueous solution - an ab initio QMCF MD simulation and large angle X-ray scattering study. *Dalton Trans.* **2012**, *41* (17), 5209−5216.

(57) Rodríguez-Maciá, P.; Galle, L. M.; Bjornsson, R.; Lorent, C.; Zebger, I.; Yoda, Y.; Cramer, S. P.; DeBeer, S.; Span, I.; Birrell, J. A. Caught in the H_{inact}: crystal structure and spectroscopy reveal a sulfur bound to the active site of an O_2-stable state of [FeFe] hydrogenase. *Angew. Chem., Int. Ed.* **2020**, *59* (38), 16786−16794.

(58) Goldet, G.; Brandmayr, C.; Stripp, S. T.; Happe, T.; Cavazza, C.; Fontecilla-Camps, J. C.; Armstrong, F. A. Electrochemical kinetic investigations of the reactions of [FeFe]-hydrogenases with carbon monoxide and oxygen: comparing the importance of gas tunnels and active-site electronic/redox effects. *J. Am. Chem. Soc.* **2009**, *131* (41), 14979−14989.

(59) Adamska-Venkatesh, A.; Krawietz, D.; Siebel, J.; Weber, K.; Happe, T.; Reijerse, E.; Lubitz, W. New redox states observed in [FeFe] hydrogenases reveal redox coupling within the H-cluster. *J. Am. Chem. Soc.* **2014**, *136* (32), 11339−11346.

(60) Lemon, B. J.; Peters, J. W. Binding of exogenously added carbon monoxide at the active site of the iron-only hydrogenase (*Cp*I) from *Clostridium pasteurianum*. *Biochemistry* **1999**, *38* (40), 12969−12973.

(61) Mebs, S.; Kositzki, R.; Duan, J.; Kertess, L.; Senger, M.; Wittkamp, F.; Apfel, U.-P.; Happe, T.; Stripp, S. T.; Winkler, M.; Haumann, M. Hydrogen and oxygen trapping at the H-cluster of [FeFe]-hydrogenase revealed by site-selective spectroscopy and QM/MM calculations. *Biochim. Biophys. Acta, Bioenerg.* **2018**, *1859* (1), 28−41.

(62) Rodríguez-Maciá, P.; Birrell, J. A.; Lubitz, W.; Rüdiger, O. Electrochemical investigations on the inactivation of the [FeFe] hydrogenase from *Desulfovibrio desulfuricans* by O_2 or light under

hydrogen-producing conditions. *ChemPlusChem* **2017**, *82* (4), 540−545.

(63) Isaac, A.; Wain, A. J.; Compton, R. G.; Livingstone, C.; Davis, J. A novel electroreduction strategy for the determination of sulfite. *Analyst* **2005**, *130* (10), 1343−1344.

(64) Siebel, J. F.; Adamska-Venkatesh, A.; Weber, K.; Rumpel, S.; Reijerse, E.; Lubitz, W. Hybrid [FeFe]-hydrogenases with modified active sites show remarkable residual enzymatic activity. *Biochemistry* **2015**, *54* (7), 1474−1483.

(65) Rodríguez-Maciá, P.; Kertess, L.; Burnik, J.; Birrell, J. A.; Hofmann, E.; Lubitz, W.; Happe, T.; Rüdiger, O. His-ligation to the [4Fe-4S] subcluster tunes the catalytic bias of [FeFe] hydrogenase. *J. Am. Chem. Soc.* **2019**, *141* (1), 472−481.

(66) Guo, M.; Sulc, F.; Ribbe, M. W.; Farmer, P. J.; Burgess, B. K. Direct assessment of the reduction potential of the $[4Fe-4S]^{1+/0}$ couple of the Fe protein from *Azotobacter vinelandii*. *J. Am. Chem. Soc.* **2002**, *124* (41), 12100−12101.

(67) Vincent, K. A.; Tilley, G. J.; Quammie, N. C.; Streeter, I.; Burgess, B. K.; Cheesman, M. R.; Armstrong, F. A. Instantaneous, stoichiometric generation of powerfully reducing states of protein active sites using Eu(II) and polyaminocarboxylate ligands. *Chem. Commun.* **2003**, No. 20, 2590−2591.

(68) Steuber, J.; Arendsen, A. F.; Hagen, W. R.; Kroneck, P. M. H. Molecular properties of the dissimilatory sulfite reductase from *Desulfovibrio desulfuricans* (Essex) and comparison with the enzyme from *Desulfovibrio vulgaris* (Hildenborough). *Eur. J. Biochem.* **1995**, *233* (3), 873−879.

(69) Harrison, G.; Curle, C.; Laishley, E. J. Purification and characterization of an inducible dissimilatory type sulfite reductase from *Clostridium pasteurianum*. *Arch. Microbiol.* **1984**, *138* (1), 72−78.

(70) Zhang, Z.; Shrager, J.; Jain, M.; Chang, C.-W.; Vallon, O.; Grossman, A. R. Insights into the survival of *Chlamydomonas reinhardtii* during sulfur starvation based on microarray analysis of gene expression. *Eukaryotic Cell* **2004**, *3* (5), 1331−1348.

(71) Baffert, C.; Kpebe, A.; Avilan, L.; Brugna, M., Chapter Three - Hydrogenases and H_2 metabolism in sulfate-reducing bacteria of the *Desulfovibrio* genus. In *Advances in Microbial Physiology*; Poole, R. K., Ed.; Academic Press: 2019; Vol. 74, pp 143−189.